Evaluation of rockfall hazard based on UAV technology and 3D Rockfall Simulations

Mustafa utlu (utlumus@gmail.com)
Bingöl Üniversitesi: Bingol Universitesi https://orcid.org/0000-0002-7508-4478
Muhammed Zeynel ÖZTÜRK
Niğde Üniversitesi: Nigde Omer Halisdemir Universitesi
Mesut Şimşek
Hatay MKÜ: Hatay Mustafa Kemal Universitesi

Research Article

Keywords: Rockfall, Hazard, RAMMS, 3D modeling, UAV.

Posted Date: April 5th, 2022

DOI: https://doi.org/10.21203/rs.3.rs-681240/v3

Abstract

In this study, the rockfall hazard in Hacıabdullah village located in the Central Anatolia region of Turkey was assessed with three-dimensional (3D) rockfall analyses based on unmanned aerial vehicle (UAV) technology using RAMMS (Rockfall software). With several rockfall disasters experienced in the village, the final event occurred in 2008, and several houses were evacuated due to rockfall risk after this event. A total of 17 hanging blocks with fall potential were identified and block dimension measurements were performed during field studies. In order to assess the rockfall hazard in the study area, digital surface model (DSM) data were obtained using high-resolution images obtained by UAV. According to dimensional values, the geometric and volumetric features of each rock were assessed close to reality with the RAMMS 3D rockfall modeling program. As a result of 3-D rockfall modelling, the maximum kinetic energy, maximum velocity, and maximum jump height of the falling blocks are reached to 3476 kJ, 23.1 m/s, and 14.57 m, respectively. The shape and volume of the blocks, as well as the slope features, rocks display differences in their runout distances after falls. A rock block with equant geometry has a runout distance of 53.1-126.9 m, whereas a rock block with flat or long geometry has a runout distance of 34-122.9 m. Rocks that do not move very far from the source area are; in other words, where the free-fall process is dominant, may significantly damage the roads. However, rolling blocks, in other words, blocks which can travel long distances from the source area, have a potential to cause great damage at the settlement areas, roads and trees. According to the hazard map, R6, R12, R13, R14, R15, R16, and R17 blocks involve high and moderate levels of risk for settlement units. R1, R4, R7, R8, R9, and R10 blocks show that the majority of them involve low risk, while a small portion is a moderate risk.

1. Introduction

Rockfalls, which are very difficult to predict in terms of occurrence time and pattern are one of the most dangerous natural disasters experienced on earth (Varnes 1978, Evans and Hungr 1993, Liu et al. 2021). Falling rocks exert significant damage on roads, settlement units, and infrastructure, in addition to causing great risk for human life (Tanarro and Munoz 2012, Lu et al. 2019, Utlu et al. 2020a). Due to the enormous speed of falling blocks, rockfalls may rapidly and suddenly occur at different angles, in nearly all conditions and different rock groups (Fityus et al. 2013, Singh et al. 2016, Gül et al. 2016). The source area of rockfalls is mostly vertical or almost vertical rock faces (Varnes 1978, Evans and Hungr 1993).

Generally, rockfalls modeling carried out by two-dimensional (2D) and three-dimensional (3D) rockfalls modeling software helps to understand of the dynamics of the rockfalls (Schober et al. 2012, Kim et al. 2015). These software have different algorithms and basis (Ansari et al. 2018). Among these models especially 2D models had been used actively, until recently. However, 3D rockfall models, which have emerged with the development of computer technologies, are much more preferred currently (Guzzetti et al. 2002, Lan et al. 2007, Bartelt et al. 2016a, Sellmeier and Thuro 2017). 3D models provide a great advantage in understanding rockfall dynamics compared to 2D models. The most important of these is to observe the rockfall trajectories on 3D surfaces, as well as to solve the hazard and risk problems such as the intersection of the transportation corridors, settlements area, infrastructure at critical points in a

quantitative way (Kim et al. 2015, Dorren and Kühne 2016). Besides, the development of remote sensing technology and remote sensing platforms such as UAV, Lidar, Radar technologies allows obtaining a 3D high-resolution surface/elevation model in a short time. In rockfall studies, 3D models offer great advantages in hazard and risk studies, especially with the use of high-resolution data. For example, simulating the desired number and shape of rock blocks and determining the possible trajectories of the modeled results are some of them (Abellán et al. 2006, Frattini et al. 2013, Kim et al. 2015, Li and Lan 2015).

Rockfall events frequently occur in Turkey, at different locations and elevations, in settlement units founded in both mountainous areas and adjacent to high slopes. Rockfall are the most frequent natural disasters after earthquakes, landslides, and floods in Turkey (Taga and Zorlu 2016, Dinçer et al. 2016, Gül et al. 2016, Aydın and Eker 2017, Geniş et al. 2017, Kayabaşı 2018, Akın et al. 2019, 2021, Utlu et al. 2021, 2020a, b). In this study, rockfall hazard was investigated in Hacıabdullah village located in Niğde province in Central Anatolia. Rockfall hazard was assessed with 3D rockfall analyses using high-resolution digital surface modeling (DSM) data based on unmanned aerial vehicle (UAV) images.

2. Study Area

Hacıabdullah village located in Niğde province in Central Anatolia which is within a valley formed by volcanic rocks on the east slopes of the Melendiz stratovolcano and is an area where intense rockfall events occur (Fig. 1a-c). Rockfalls are mostly experienced on high-slope areas located north of the village (Fig. 1d) and the village is located under a steep slope with an inclination of 90°. The inclination of the terrain where rockfall events occur vary between 23 and 90° and the area has a convex profile. The steep slope which is the rockfall source in the study area is composed of volcanic rocks containing vertical cooling joints triggering many rockfall events not only in the past but also recently (Fig. 2). The study area has semi-arid climate features shown by the letters “BSk” according to the Köppen-Geiger climate classification (Öztürk et al. 2017). Freeze-thaw processes occurring especially during the winter season, gravity on high slope areas, and the general lithology of the study area containing volcanic rocks with heavily jointed structure play dominant roles in triggering rockfall events.

According to a report by the Ministry of Interior Disaster and Emergency Management Presidency (AFAD), Hacıabdullah village has experienced several rockfall events from 1957 to the present day on different dates. According to the AFAD report, 6 severe rockfall events took place on 05/04/1957, 26/06/1963, 13/09/1974, 21/03/1983, 13/11/2007, and 03/03/2008. In the report from 1957, the decision was made to evacuate 85 families at risk from rockfalls; however, the local public had not implemented this decision. A report in 1963 stated that 92 households were damaged by both rockfalls and floods. In 1974, 12 houses were affected by rockfalls. In 2007, it was recommended that 50 houses with rockfall risk be moved. During a rockfall occurring in 2008, 2 houses were damaged by rockfalls (AFAD, 2011; Fig. 2).

3. Datasets And Processing

Accurate analysis is required due to the high hazard and risk status of rockfalls. From this aspect, modeling studies have great importance (Mary Vick et al. 2019). For rockfall modelling studies, geomorphometric approaches and modelling based on high-resolution DSM data provide more accurate and sensitive results (Loye et al. 2009, Zhang et al. 2019, Pérez-Rey et al. 2019, Francioni et al. 2020, Rodriguez et al. 2020, Akın et al. 2021). Within this scope, UAVs offer significant advantages in producing DSM and orthophoto data for large areas in a short duration and gain great importance for monitoring the distribution of natural disasters, especially, in spatial and temporal terms (Feng and Röshoff 2004, Abellán et al. 2006, Armesto et al. 2009, Alejano et al. 2013, Giordan et al. 2015). High-resolution DSM and orthophoto data are very effective for accurate and sensitive trajectory modeling and the detection of source zones in rockfall prone areas. For this reason, rockfall studies in recent years have moved beyond traditional methods (Colomina and Molina 2014, Boccardo et al. 2015, Gomez and Purdie 2016, Manconi et al. 2019) and begun to use high-resolution DSM and orthophoto images obtained with UAVs (Matasci et al. 2015, Török et al. 2017, Byrne 2018, Manconi et al. 2019).

3.1. UAV Survey and Photogrammetric processing

In this study, a DJI Phantom 4 Advanced UAV was used to produce high-resolution orthophoto and digital surface models for rockfall modeling. The general flowchart followed when producing this data is given in Fig. 3.

Preparations for flight height, scanning width and stereo image matching proportions were completed with Pix4dcapture software for the study area. With the aim of producing DSM and orthophoto data with good quality and sensitivity, 40 ground control points (GCP) were placed with D-GPS before the flight. Five parallel flights were made at 100 meters height, and 621 stereo aerial photographs were obtained with 70% overlap ratio (Fig. 4a-b). Processing of these images was performed using the Pix4d trial version. Eventually, point cloud data with a 3.03 cm resolution were obtained after the photogrammetric processing of orthophoto images with low (1.4 cm) RMSE error (Fig. 4c-d).

3.2. Evaluation of the quality of elevation data of DSMs

There are some errors when DSM data is obtained using different platforms. These errors are caused by the structure of the land surface and land use/cover features.

One of these errors is the vertical error rate (Ajayi et al. 2017, Coveney and Roberts 2017). Ground control points (GCPs) and checkpoints (CPs) are used to fix these errors during collecting stereo images by UAV. In order to understand the vertical accuracy error rate, CP data is also collected in addition to the GCP data. Determining the vertical accuracy rate in DSM data is important for the performance of the study and the precision of the results (Tamminga et al. 2015).

In this respect, using 35 checkpoints in the study area, the vertical accuracy rate of the DSM data root mean square error (RMSE, Formula 1), mean square error (MSE, Formula 2), mean absolute deviation

(MAD, Formula3) and mean absolute tested with percentage error (MAPE, Formula 4) (Tamminga et al. 2015, Akturk and Altunel 2019). These formulas are expressed as,

$$\mathrm{RMSE} = \sqrt{\frac{\sum_{t=1}^{n} (A_t - F_t)^2}{n}} \quad (1)$$

$$\mathrm{MSE} = \frac{\sum_{t=1}^{n} (A_t - F_t)^2}{n} \quad (2)$$

$$\mathrm{MAD} = \frac{\sum_{t=1}^{n} |A_t - F_t|}{n} \quad (3)$$

$$\mathrm{MAPE} = \frac{\sum_{t=1}^{n} \left| \frac{A_t - F_t}{A_t} \right|}{n} \times 100 \quad (4)$$

The results obtained according to the specified formulas are given in Table 1. Accordingly, the error rates of the DSM data are MAD: 0.169, MSE: 0.066, RMSE: 0.258, MAPE: 0.01 cm. Accordingly, DSM data was obtained with a low vertical accuracy error rate.

Table 1
The vertical accuracy results of the DSM data based on different statistical parameters using RMSE, MSE, MAD, MAPE.

Check point	Actual Elevations	Forecast Elevations	Error	Absolute Value of Error	Square of Error	Absolute Values of Errors Divided by Actual Values.
	At	Ft	At -Ft	| At -Ft|	(At - Ft)^2	| (At -Ft)/At|
1	1630.25	1630.10	-0.15	0.150	0.023	0.0001
2	1638.29	1638.13	-0.16	0.160	0.026	0.0001
3	1637.38	1638.00	0.62	0.620	0.384	0.0004
4	1628.94	1628.87	-0.07	0.070	0.005	0.0000
5	1619.62	1619.55	-0.07	0.070	0.005	0.0000
6	1633.70	1632.93	-0.77	0.770	0.593	0.0005
7	1596.07	1595.99	-0.08	0.080	0.006	0.0001
8	1590.10	1590.09	-0.01	0.010	0.000	0.0000
9	1593.89	1593.85	-0.04	0.040	0.002	0.0000
10	1589.94	1589.85	-0.09	0.090	0.008	0.0001
11	1587.47	1588.00	0.53	0.530	0.281	0.0003
12	1593.24	1593.13	-0.11	0.110	0.012	0.0001
13	1631.93	1631.87	-0.06	0.060	0.004	0.0000
14	1569.82	1569.78	-0.04	0.040	0.002	0.0000
15	1612.38	1612.30	-0.08	0.080	0.006	0.0000
16	1566.89	1566.78	-0.11	0.110	0.012	0.0001
17	1622.20	1623.00	0.80	0.800	0.640	0.0005
18	1595.68	1595.60	-0.08	0.080	0.006	0.0001
19	1562.14	1562.00	-0.14	0.140	0.020	0.0001
20	1574.44	1574.32	-0.12	0.120	0.014	0.0001
21	1571.70	1571.60	-0.10	0.100	0.010	0.0001
22	1589.67	1589.60	-0.07	0.070	0.005	0.0000
23	1566.96	1567.10	0.14	0.140	0.020	0.0001
24	1599.51	1599.40	-0.11	0.110	0.012	0.0001

Check point	Actual Elevations	Forecast Elevations	Error	Absolute Value of Error	Square of Error	Absolute Values of Errors Divided by Actual Values.
25	1612.30	1612.20	-0.10	0.100	0.010	0.0001
26	1592.02	1591.99	-0.03	0.030	0.001	0.0000
27	1547.38	1547.70	0.32	0.320	0.102	0.0002
28	1556.64	1556.50	-0.14	0.140	0.020	0.0001
29	1586.68	1586.60	-0.08	0.080	0.006	0.0001
30	1576.71	1576.50	-0.21	0.210	0.044	0.0001
31	1583.12	1583.00	-0.12	0.120	0.014	0.0001
32	1553.27	1553.20	-0.07	0.070	0.005	0.0000
33	1548.69	1548.60	-0.09	0.090	0.008	0.0001
34	1555.24	1555.13	-0.11	0.110	0.012	0.0001
35	1552.49	1552.40	-0.09	0.090	0.008	0.0001
	Totals		-1.090	5.910	2.326	0.004
	N	35				
	MAD	**MSE**	**RMSE**	**MAPE**		
	0.169	0.066	0.258	0.01		

3.3. Discontinuity analysis based on point cloud data

Discontinuity analysis, which is used in the identification of fracture and crack joints in rock surface, is important to understand behavior of the blocks. Discontinuities are explained by creating contour diagrams depending on the angle of the extension of the cracks and fractures in the rock units with the north (Zhang 2006, Riquelme et al. 2018). In recent years, LIDAR, TLS, and UAV platforms, which are actively used and highly preferred in the creation of digital surface data (DSM-DTM) and play a major role in the creation of discontinuities (Dewez et al. 2016, Riquelme et al. 2017, 2018, Valkaniotis et al. 2018). Discontinuities were performed in 3 part of the high slope source zone in this study (Fig. 5) and discontinuities were analyzed based on UAV-3D Point cloud data using qFacet plugin that allows to extract characteristics of the rock surface such as planar facets and their orientation and distance (Dewez et al. 2016, Valkaniotis et al. 2018). The mean dip angel and dip direction for the study area gives a similar result based on high-density point cloud datasets (Fig. 5. 1a-2b-3c). Besides, the discontinuity results obtained from 3 different locations gave very similar values. Accordingly, the obtained orientations generally refer to the areas corresponding to the vertical cooling cracks due to the lithology of the area. The general values obtained accordingly show that there are 3 main discontinuity surfaces

represents Fig. 5b-c-d and the mean dip direction (°) of these surfaces is between 190–208°, on the other hand, the dip angle (°) values are between 33–35° (Fig. 5 and Table 2).

Table 2
The summary of the discontinuities in the study area based on qFacet plugins

Section	No. of planes	Mean		
		Dip (°)	Dip direction (°)	RMSE
1	7602	30	190	0.143
2	4269	35	203	0.123
3	2034	33	208	0.124

3.4. Block geometries

In the study area, which is at high risk of rockfall, the source zones of blocks generally correspond to cooling cracks located on steep slopes of cliffs (Figure. 2). To identify blocks that have potential falling risks, field studies were performed and 17 blocks were identified (Fig. 6). The height, width, and length were measured for each block and according to these values each rock is modelled in 3D RAMMS: ROCKFALL 1.6. 70 module software (Table 3). While 10 of the modeled rock blocks (R1-R2-R4-R6-R7-R10-R11-R15-R16-R17) have equant and real-equant geometry, 5 rocks (R3-R9-R12-R13-R14) have long and real-long geometry and R5-R8 blocks have flat geometry (Fig. 7). RAMMS software provides a great advantage for accurate and high-quality modeling of rocks with different shapes and volumes measured in field studies (Mary Vick et al. 2019) and takes into account the real size of blocks (Dorren and Kühne 2016, Torsello et al. 2021).

Table 3
Properties of the simulated rocks

No	X (length) m	Y (width) m	Z (height) m	Volume m^3	Mass kg	Rock shape
R1	3.2	2.5	1.5	7.96	21485.4	Equant
R2	2.0	1.8	1.0	1.545	4172.5	Equant
R3	1.5	1.6	1.2	0.719	1941.7	Real long
R4	1.42	1.23	1.0	0.95	2565.2	Real Equant
R5	1.2	1.4	0.8	0.925	2497.8	Real Flat
R6	1.5	1.25	1.0	1.124	3035.6	Equant
R7	1.5	1.25	1.0	1.124	3035.6	Equant
R8	1.22	1.17	1.0	0.687	1856	Real Flat
R9	0.96	1.16	0.98	0.464	1253.5	Real Long
R10	1.42	1.23	1.0	0.950	2565.2	Real Equant
R11	1.42	1.23	1.0	0.950	2565.2	Real Equant
R12	1.15	1.49	1.0	0.698	1.885	Real Long
R13	3.24	1.62	2.23	0.524	1414.1	Real Long
R14	1.56	2.01	1.35	0.719	1941.7	Real Long
R15	1.42	1.23	1.0	0.950	2565.2	Real Equant
R16	1.61	1.34	1.07	1.124	3035.6	Equant
R17	2.18	2.34	1.87	1.242	3352.4	Real Equant

3.5. Rockfall simulations

A range of rockfall models were developed in order to assess rockfalls in terms of dynamics, trajectories, kinetic energy, velocity and jump height and many other aspects (Azzoni et al. 1995, Dorren 2003, Volkwein et al. 2011, Frattini et al. 2012, Žabota et al. 2021, Liu et al. 2021). RAMMS, CONEFALL, STONE, Georock, Rockyfor3D, FlowR and Rotomap produce two-dimensional (2D) and 3D rockfall models based on different algorithms and GIS for spatial analysis (Guzzetti et al. 2002, Jaboyedoff and Labiouse 2011, Topal et al. 2012, Bartelt et al. 2016a). 3D rockfall simulations are performed on 3D surface/elevation models to determine rockfall trajectories and runout zones (Dorren 2003). Results obtained from this modeling provide advantages in producing hazard maps for rockfall susceptibility, protection, vulnerability, failure and distribution of rockfalls (Vo 2015; Bonneau et al. 2018; Sarro et al. 2018; Singh et al. 2018; Sazid 2019). For this reason, implementing the necessary protective systems (fences, ditches

and forests etc.) as a result of modeling by identifying these blocks and performing the necessary measurements may prevent these hazards and risks (Piacentini and Soldati 2008).

In this study, after determining the geometric and volumetric properties of these blocks with very different shapes and volumes, 3D rockfall analyses were executed with the RAMMS: Rockfall software which is a GIS-based rockfall simulation program (Leine et al. 2014; Bartelt et al. 2016a). In the rockfall modeling process, a range of data inputs are required in addition to modeling obtained linked to DSM data. These inputs include features like plant cover (open, dense, etc.), terrain types (hard, extra hard, medium, soft, medium soft, etc.) and block types (flat, equitant, round, etc.) for blocks or source zone areas to be modelled by the RAMMS program (Vo 2015). For rockfall modeling in the RAMMS program, DSM data with resolution from 1–10 m is sufficient. For this reason, DSM data with cm-resolution was rescaled to 1-meter resolution to obtain the format for use in modeling. Considering the volcanic rocks in the field, the terrain type was selected as hard terrain, covered with very sparse plant cover (Fig. 4c). Besides, the friction parameters (Table 4) were determined based on terrain type that account for; “Rocks jump over ground, includes different size of blocks and absence of the vegetation” (Bartelt et al. 2016b).

Table 4
The friction parameters of the simulated rockfalls (Bartelt et al. 2016b).

Material strength	Material weakening	Rock ejection	Material behaviour
μ min	μ min	β	κ	v
0.55	2	185	3	0.4

3.6. Rockfall Hazard Index

Rockfall Hazard Index (RHI) method was employed for the hazard mapping of rockfalls (Crosta and Agliardi 2003). In this method, the kinetic energy, jump height and block count parameters are taken into consideration which was determined through the RAMMS program in this study. These basic parameters are reclassified within the scope of hazards. During the reclassification, the classification values of Crosta and Agliardi (2003) were used. Necessary classifications for kinetic energy, jump height and block count values are presented in Table 5. For calculation of block count value, the c/(5*n) formula was used and then reclassification was performed. As we can see in the formula, c represents rockfall count, and n represents the number of blocks from each cell value. The values obtained as a result of the modeling of the rock blocks were evaluated separately for each block based on RHI. The values obtained were separately calculated for reach rockfall model with the results of classification of the 3 parameters combined to identify high-moderate-low hazard areas.

Table 5
Classification of parameters according to the Rockfall Hazard Index method (Crosta and Agliardi, 2003).

Class	Block count (local scale)	Kinetic energy (kJ)	Jump height (m)
1	< 0.01	≤ 700	≤ 4
2	0.01–0.1	700–2500	4–10
3	> 0.1	≥ 2500	≥ 10

4. Results

According to the dimension of blocks determined during the field studies, heights vary from 0.8 to 2.23 m, lengths from 0.96 to 3.2 m, and widths of 1.16 to 2.5 m (Fig. 7). As a result of these dimensions, the volume of blocks was calculated in between 0.46 and 7.96 m^3, while block mass was calculated to be in a range of 214.48 to 1253 kg. The block shapes were identified as equant, real long, real equant, and real flat in the RAMMS program, a total of 100 throws for each block at 17 different release locations were modeled and the kinetic energy (kJ), velocity (m/s), jump height (m) and Rockfall Hazard Index were determined.

As a result of the shape and volume of the blocks, as well as the slope features, rocks display differences in their runout distances after falls. Model results showed maximum kinetic energy values (3476.8 kJ), seeing that on equant geometry of blocks, while low kinetic energy values (90.6 kJ) seeing that on flat and long geometry of blocks (Fig. 8). With 90.6 kJ, the lowest value is found in R5 with flat geometry, while the highest value is found in R1 with equant geometry. The rock velocity values vary depending on the topography of the field and the slope. The velocity values between 8 and 23.1 m/s reach. The maximum and minimum velocities observed in R11 and R13, respectively. In addition to these values, while equant shaped rock blocks exhibit a velocity value between 10-23.1 m/s, flat and long blocks show a velocity value between 8.74 and 19.93 m/s. Jump height values range between 1.99 and 14.5 m. Equant blocks have values ranging from 3.4–14.5 m, while long and flat blocks have values between 1.99 and 7.8 m. As seen for blocks R1, R4, R6, R7, R8, R9, R10, R11, R12, R14, R15, R16, and R17 represent equant features that involve different size and volume are present different run out distance based onto the geometry of the blocks. Apart from this, R12 block has a continuous slope profile; however, the block could not progress a long distance due to the different shape (real long). A rock block with equant geometry has a runout distance of 53.1-126.9 m, whereas a flat or long geometry has a runout distance of 34-122.9 m. In the case of the rock block R8, whose value is 122.9 m, the trajectory was carried over long distances due to the continuous steep slopes (Fig. 19). It should be noted that the residential houses shown in Fig. 10 are mostly demolished and thus some trajectories are rolling over the remnants of these buildings.

Just as the geometric shapes of blocks and slope features of the area affect the kinetic energy, they also control the block velocity and the jump height. Generally, high velocity and jump height values are obtained at the areas where kinetic energy reaches maximum levels. As a result of modeling of 17 different blocks, maximum velocity values are between 8.17 and 23.1 m/s, maximum jump height vary from 1.99 m to 14.5 m (Table 6). The block with lowest kinetic energy, jump height and velocity value appeared to be block number R5 with a flat geometry (Table 3).

Using rockfall modeling, it is found that most of the falling blocks surpass the houses due to their properties that are compatible with the topography and geomorphologic characteristics of the area. These houses are located as a so-called amphitheater and spread in accordance with the topography in places where the slope decreases (Fig. 9). As seen Fig. 9 some part of the settlements has been affected by rockfall events that damaged or demolished the houses. The jump height values obtained by rockfall modeling indicate that the blocks may jump over the settlement units under suitable topographic conditions and cover long distances damaging houses and walls. These residential areas are affected more by rockfall events due to the distribution of the settlements and their geographic location, causing more damage (Fig. 9). As can be seen from the modeling results, while a total of 11 blocks exceed the houses (R1-R7-R8-R9-R10-R11-R12-R13-R15-R16-R17), only 6 blocks (R2-R3-R4-R5-R6-R14) are damped before reaching the houses due to their low kinetic energy and jump height values.

4.1. Rockfall Hazard Assessment

The rockfall trajectories determined by means of rockfall simulations point out a significant risk for the investigated settlement. The rockfall parameters of 17 blocks determined via RAMMS software by are summarized in Table 6. Blocks falling from vertical steep slopes generally stop on the roads before reaching the settlement units. However, apart from R2, R3 and R5, a total of 14 different blocks may damage residential units in the study area. These blocks have very high-risk due to being transported over long distances. It appears they may cause great damage and even loss of life due to high energy, velocity and jump height.

Table 6
Rockfall parameters obtained by 3D rockfall modeling (H: House, T: Tree, R: Road)

No	Max. kinetic energy (kJ)	Max. velocity (m/s)	Max. jump height (m)	Max. runout distance (m)	Element at risk
R1	3476.8	16.73	5.25	126.9	H,T,R
R2	1183.5	14.53	4.25	81.6	T,R
R3	160.6	10.15	2.27	59.8	T,R
R4	383.1	16.46	5.75	112.5	H,T,R
R5	90.6	8.17	1.99	75.8	No contact
R6	581	17.9	9.02	94	H,T
R7	131	17.19	8.71	55.07	Abandoned H
R8	397.5	19.93	7.83	122.9	H,T,R
R9	185.2	16.51	6.84	85.2	H,T,R
R10	285.4	13.71	6.05	84	H,T,R
R11	701	23.1	14.57	90.1	H,T,R
R12	166	12.06	4.1	56.6	H,T
R13	630	8.74	4.55	34.5	H
R14	441	13	6.23	44.8	H
R15	312	14.63	6.42	65.3	H,T,R
R16	257.4	10.61	3.04	53.1	H,T
R17	1737.6	16.05	10.1	69.7	H,T,R

To map the hazard of rockfalls, Crosta and Agliardi (2003) used the "Rockfall Hazard Index" (RHI). In this study, the RAMMS program was used to determine the kinetic energy, jump height, and block count parameters to create rockfalls hazard map. Using the hazard map, modeling of rocks R6, R12, R13, R14, R15, R16, and R17 indicates that settlement areas constitute most of the high and moderate risk areas. Modeling of blocks R1, R4, R7, R8, R9 and R10 show the majority involve low hazard, while a small portion involve moderate degree of hazard (Fig. 10).

Conclusions

In this study, rockfall risks in Hacıabdullah village where rockfall events occur continuously were assessed using high-resolution DMS, field measurements, and 3D rockfall simulations. Based on RAMMS analysis, the kinetic energy varies between 90.6 and 3476 kJ, the velocity between 8.17 and 23.1 m/s, and the jump height between 1.99 and 14.57 meters. These values show variation according to the

general slope values for the study area and trajectory of the modelled blocks the slope profile and geomorphology of the study area, and the geometry and volume of the blocks. Rock blocks may travel very long distances in regions with slope values below 46°, while blocks stop on slope breaks without traveling long distances when slope values are from 46–90°. Some of the results rockfalls modelling shows the trajectories that channelled into valleys ended within the valley, while some of the results rockfalls that found on ridges show large areas are threatened. As a result of the shape and volume of the blocks, as well as the slope features, rocks display differences in their runout distances after falls. A rock block with equant geometry has a runout distance of 53.1-126.9 m, whereas a flat or long geometry has a runout distance of 34-122.9 m. It should be noted that the residential houses are mostly demolished and thus some trajectories are rolling over the remnants of these buildings. According to the hazard map, R6, R12, R13, R14, R15, R16 and R17 involve high and moderate levels of risk for settlement units. R1, R4, R7, R8, R9, and R10 show that the majority of them involve low risk, while a small portion is moderate risk. Taking the necessary precautions for the determined risk areas has vital importance due to the frequent experience of rockfalls in the area. The model outcomes should be considered when taking the necessary precautions. In conclusion, in Hacıabdullah village where rockfall events are actively experienced, risk for settlement areas and the spatial distribution of the possible risk were accurately revealed by field study results and rockfall models completed with a high-resolution digital elevation model produced with the aid of a UAV. These results have great importance in terms of taking the necessary precautions based on rockfall hazard maps.

Declarations

Ethical Statements

Conflicts of Interest: The author declares no conflict of interest.

Funding:

This research received no external funding.

References

1. Abellán A, Vilaplana JM, Martínez J (2006) Application of a long-range Terrestrial Laser Scanner to a detailed rockfall study at Vall de Núria (Eastern Pyrenees, Spain). Int J Rock Mech Min Sci & Geomech 88:136–148
2. Ajayi OG, Salubi AA, Angbas AF, Odigure MG (2017) Generation of accurate digital elevation models from UAV acquired low percentage overlapping images
3. Akın M, Dinçer İ, Ok A, Orhan A, Akin MK, Topal T (2021) Assessment of the effectiveness of a rockfall ditch through 3-D probabilistic rockfall simulations and automated image processing. Eng Geol 283:106001

4. Akın M, Dinçer İ, Orhan A, Ok A, Akin M, Topal T (2019) Evaluation of the Performance of a Rockfall Ditch by 3-Dimensional Rockfall Analyses: Akköy (Ürgüp) Case. Jeoloji Muhendisligi Dergisi 43:211–232
5. Akturk E, Altunel AO (2019) Accuracy assessment of a low-cost UAV derived digital elevation model (DEM) in a highly broken and vegetated terrain. Measurement 136:382–386
6. Alejano LR, García-Cortés S, García-Bastante F, Martínez-Alegría R (2013) Study of a rockfall in a limy conglomerate canyon (Covarrubias, Burgos, N. Spain). Environ Earth Sci 70:2703–2717
7. Ansari MK, Ahmad M, Singh R, Singh TN (2018) 2D and 3D rockfall hazard analysis and protection measures for Saptashrungi Gad Temple, Vani, Nashik, Maharashtra – A case study. J Geol Soc India 91:47–56
8. Armesto J, Ordóñez C, Alejano L, Arias P (2009) Terrestrial laser scanning used to determine the geometry of a granite boulder for stability analysis purposes. Geomorphology 106:271–277
9. Aydın A, Eker R (2017) Kaya yuvarlanmalarından etkilenen orman alanlarının belirlenmesi: İnebolu örneği. İstanbul Üniversitesi Orman Fakültesi Dergisi 67:136–149
10. Azzoni A, La Barbera G, Zaninetti A (1995) Analysis and prediction of rockfalls using a mathematical model. Int J Rock Mech and Min Sci and 32:709–724
11. Baillifard F, Jaboyedoff M, Sartori M (2010) Rockfall hazard mapping along a mountainous road in Switzerland using a GIS-based parameter rating approach. Nat Hazards Earth Syst Sci 3:435–442
12. Bartelt P, Bieler C, Bühler Y, Christen M, Christen M, Dreier L, Gerber W, Glover J, Schneider M, Glocker C, Leine R, Schweizer A (2016a) RAMMS::ROCKFALL User Manual v1.6:102.
13. Bartelt P, Gerber W, Christen M, Bühler Y (2016b) Modeling rockfall trajectories with non-smooth contact/impact mechanics.Pages203–211 13th Congress Interpraevent 2016.
14. Berger F, Rey F (2004) Mountain protection forests against natural hazards and risks: New french developments by integrating forests in risk zoning. Nat Hazards 33:395–404
15. Boccardo P, Chiabrando F, Dutto F, Tonolo FG, Lingua A (2015) UAV Deployment Exercise for Mapping Purposes: Evaluation of Emergency Response Applications. Sensors 15:15717–15737
16. Bonneau DA, Hutchinson DJ, Difrancesco P, Coombs M, Sala Z (2018) 3-Dimensional Rockfall Shape Back-Analysis: Methods and Implications:1–35
17. Byrne K (2018) Digital Morphometry Applied to Geo-Hazard Risk Assessment: A Case Study from Germany. Technische Universitat Dresden. Faculty of Environmental Sciences, Institute for Cartography, Master of Science
18. Colomina I, Molina P (2014) Unmanned aerial systems for photogrammetry and remote sensing: A review. ISPRS J Photogrammetry Remote Sens 92:79–97
19. Coveney S, Roberts K (2017) Lightweight UAV digital elevation models and orthoimagery for environmental applications: data accuracy evaluation and potential for river flood risk modelling. Int J Remote Sens 38:3159–3180

20. Crosta GB, Agliardi F (2003) A methodology for physically based rockfall hazard assessment. Nat Hazards Earth Syst Sci 3:407–422
21. Dewez TJB, Girardeau-Montaut D, Allanic C, Rohmer J (2016) Facets: A cloudcompare plugin to extract geological planes from unstructured 3d point clouds
22. Dhiman RK, Thakur M (2021) Rockfall Hazard Assessment Using RAMMS for the SE Facing Escarpment of Manikaran, Himachal Pradesh, India. Recent Technologies for Disaster Management and Risk Reduction, pp 57–74
23. Dinçer İ, Orhan A, Frattini P, Crosta GB (2016) Rockfall at the heritage site of the Tatlarin Underground City (Cappadocia, Turkey). Nat Hazards 82:1075–1098
24. Dorren LKA (2003) A review of rockfall mechanics and modelling approaches. Prog Phys Geogr 27:69–87
25. Dorren LKA, Maier B, Putters US, Seijmonsbergen AC (2004) Combining field and modelling techniques to assess rockfall dynamics on a protection forest hillslope in the European Alps. Geomorphology 57:151–167
26. Dorren LKA, Seijmonsbergen AC (2003) Comparison of three GIS-based models for predicting rockfall runout zones at a regional scale. Geomorphology 56:49–64
27. Dorren L, Kühne R (2016) Comparing the 3D rockfall simulation models Rockyfor3D and RAMMS::. ROCKFALL at a case study site in Switzerland
28. Einstein HH, Veneziano D, Baecher GB, O'Reilly KJ (1983) The effect of discontinuity persistence on rock slope stability. Int J Rock Mech and Min Sci and 20:227–236
29. Evans SG, Hungr O (1993) The assessment of rockfall hazard at the base of talus slopes. Can Geotech J 30:620–636
30. Feng QH, Röshoff K (2004) In-situ mapping and documentation of rock faces using a full-coverage 3d laser scanning technique. Int J Rock Mech Min Sci 41:1–6
31. Fityus SG, Giacomini A, Buzzi O (2013) The significance of geology for the morphology of potentially unstable rocks. Eng Geol 162:43–52
32. Francioni M, Antonaci F, Sciarra N, Robiati C, Coggan J, Stead D, Calamita F (2020) Application of Unmanned Aerial Vehicle Data and Discrete Fracture Network Models for Improved Rockfall Simulations. Remote Sens 12:2053
33. Frattini P, Crosta GB, Agliardi F (2012) Rockfall characterization and modeling. In: Clague JJ, Stead D (eds) Landslides. Cambridge University Press, Cambridge, pp 267–281
34. Frattini P, Crosta GB, Agliardi F, Imposimato S (2013) Landslide Science and Practice. In: Margottini C, Canuti P, Sassa K (eds) Landslide Science and Practice; Challenging Calibration in 3D Rockfall Modelling. Springer, Berlin Heidelberg, Berlin, Heidelberg, pp 169–175
35. Geniş M, Sakız U, Çolak Aydıner B (2017) A stability assessment of the rockfall problem around the Gökgöl Tunnel (Zonguldak, Turkey). Bull Eng Geol Environ 76:1237–1248

36. Giordan D, Manconi A, Facello A, Baldo M, Anese F, Allasia P, Dutto F, Dell'Anese F, Allasia P, Dutto F (2015) Brief Communication: The use of an unmanned aerial vehicle in a rockfall emergency scenario. Nat Hazards Earth Syst Sci 15:163–169
37. Gomez C, Purdie H (2016) UAV- based Photogrammetry and Geocomputing for Hazards and Disaster Risk Monitoring – A Review.Geoenvironmental Disasters3
38. Gül M, Özbek A, Karacan E (2016) Rock fall hazard assessment in Asar Hill, ancient Mabolla City, Mugla—SW Turkey. Environ Earth Sci 75:1310
39. Guzzetti F, Crosta G, Detti R, Agliardi F (2002) STONE: A computer program for the three-dimensional simulation of rock-falls. Comput Geosci 28:1079–1093
40. Jaboyedoff M, Labiouse V (2011) Technical note: Preliminary estimation of rockfall runout zones. Nat Hazards Earth Syst Sci 11:819–828
41. Kayabaşı A (2018) The assesment of rockfall analysis near a railroad: a case study at the Kızılinler village of Eskişehir, Turkey. Arab J Geosci 11:800
42. Kim DH, Gratchev I, Berends J, Balasubramaniam A (2015) Calibration of restitution coefficients using rockfall simulations based on 3D photogrammetry model: a case study. Nat Hazards 78:1931–1946
43. Lan H, Derek Martin C, Lim CH (2007) RockFall analyst: A GIS extension for three-dimensional and spatially distributed rockfall hazard modeling. Comput Geosci 33:262–279
44. Leine RI, Schweizer A, Christen M, Glover J, Bartelt P, Gerber W (2014) Simulation of rockfall trajectories with consideration of rock shape. Page Multibody System Dynamics
45. Li L, Lan H (2015) Probabilistic modeling of rockfall trajectories: a review. Bull Eng Geol Environ 74:1163–1176
46. Liu G, Li J, Wang Z (2021) Experimental Verifications and Applications of 3D-DDA in Movement Characteristics and Disaster Processes of Rockfalls. Rock Mechanics and Rock Engineering
47. Loye A, Jaboyedoff M, Pedrazzini A (2009) Identification of potential rockfall source areas at a regional scale using a DEM-based geomorphometric analysis. Nat Hazards Earth Syst Sci 9:1643–1653
48. Lu G, Caviezel A, Christen M, Demmel SE, Ringenbach A, Bühler Y, Dinneen CE, Gerber W, Bartelt P (2019) Modelling rockfall impact with scarring in compactable soils. Landslides 16:2353–2367
49. Manconi A, Ziegler M, Blöchliger T, Wolter A (2019) Technical note: optimization of unmanned aerial vehicles flight planning in steep terrains. Int J Remote Sens 40:2483–2492
50. Mary Vick L, Zimmer V, White C, Massey C, Davies T (2019) Significance of substrate soil moisture content for rockfall hazard assessment. Nat Hazards Earth Syst Sci 19:1105–1117
51. Matasci B, Jaboyedoff M, Loye A, Pedrazzini A, Derron MH, Pedrozzi G (2015) Impacts of fracturing patterns on the rockfall susceptibility and erosion rate of stratified limestone. Geomorphology 241:83–97

52. Öztürk MZ, Çetinkaya G, Aydın S (2017) Köppen-Geiger İklim Sınıflandırmasına Göre Türkiye'nin İklim Tipleri.Coğrafya Dergisi:17–27(In Turkish).
53. Pérez-Rey I, Riquelme A, González-deSantos LM, Estévez-Ventosa X, Tomás R, Alejano LR (2019) A multi-approach rockfall hazard assessment on a weathered granite natural rock slope. Landslides 16:2005–2015
54. Piacentini D, Soldati M (2008) Application of empiric models for the analysis of rock-fall runout at a regional scale in mountain areas: Examples from the dolomites and the northern apennines (Italy). Geografia Fisica e Dinamica Quaternaria 31:215–223
55. Riquelme A, Cano M, Tomás R, Abellán A (2017) Identification of Rock Slope Discontinuity Sets from Laser Scanner and Photogrammetric Point Clouds: A Comparative Analysis. Procedia Eng 191:838–845
56. Riquelme A, Tomás R, Cano M, Pastor JL, Abellán A (2018) Automatic Mapping of Discontinuity Persistence on Rock Masses Using 3D Point Clouds. Rock Mech Rock Eng 51:3005–3028
57. Rodriguez J, Macciotta R, Hendry MT, Roustaei M, Gräpel C, Skirrow R (2020) UAVs for monitoring, investigation, and mitigation design of a rock slope with multiple failure mechanisms—a case study. Landslides 17:2027–2040
58. Sarro R, Carlos J, Mar R (2018) Rockfall Simulation Based on UAV Photogrammetry Data Obtained during an Emergency Declaration:Application at a Cultural Heritage Site. Remote Sensing
59. Sazid M (2019) Analysis of rockfall hazards along NH-15: A case study of Al-Hada road. Int J Geo-Engineering 10:1–13
60. Schober A, Bannwart C, Keuschnig M (2012) Rockfall modelling in high alpine terrain - validation and limitations / Steinschlagsimulation in hochalpinem Raum - Validierung und Limitationen. Geomech Tunn 5:368–378
61. Sellmeier B, Thuro K (2017) Comparison of two 3D rockfall codes on behalf of a case study in the Bavarian Alps. Geomechanik und Tunnelbau 10:15–23
62. Singh A, Pal S, Kanungo DP (2018) Site-Specific Vulnerability Assessment of Buildings Exposed to Rockfalls. Renewable Energy and its Innovative Technologies:1–11
63. Singh PK, Kainthola A, Panthee S, Singh TN (2016) Rockfall analysis along transportation corridors in high hill slopes. Environ Earth Sci 75:1–11
64. Taga H, Zorlu K (2016) Assessment of rockfall hazard on the steep-high slopes: Ermenek (Karaman, Turkey). Natural Hazards and Earth System Sciences Discussions:1–32
65. Tamminga A, Hugenholtz C, Eaton B, Lapointe M (2015) Hyperspatial Remote Sensing of Channel Reach Morphology and Hydraulic Fish Habitat Using an Unmanned Aerial Vehicle (UAV): A First Assessment in the Context of River Research and Management. River Res Appl 31:379–391
66. Tanarro LM, Munoz J (2012) Rockfalls in the Duratón canyon, central Spain: Inventory and statistical analysis. Geomorphology 169–170:17–29

67. Topal T, Akın MK, Akın M (2012) Rockfall hazard analysis for an historical Castle in Kastamonu (Turkey). Nat Hazards 62:255–274
68. Török Á, Barsi Á, Bögöly G, Lovas T, Somogyi Á, Görög P (2017) Slope stability and rock fall hazard assessment of volcanic tuffs using RPAS and TLS with 2D FEM slope modelling.Natural Hazards and Earth System Sciences Discussions:1–30
69. Torsello G, Vallero G, Castelli M (2021) The role of block shape and slenderness in the preliminary estimation of rockfall propagation. IOP Conference Series: Earth and Environmental Science 833:012177
70. Utlu M, Öztürk MZ, Şimşek M (2020a) Rockfall analysis based on UAV technology in Kazıklıali Gorge, Aladağlar (Taurus Mountains, Turkey). Int J Environ Geoinformatics 7:239–251
71. Utlu M, Öztürk MZ, Şimşek M (2020b) Emli Vadisi'ndeki (Aladağlar) Talus Depolarının Kantitatif Analizlere Göre İncelenmesi. In: Birinci S, Kıvanç Ç, Kaymaz, Kızılkan Y (eds) COĞRAFİ PERSPEKTİFLE DAĞ VE DAĞLIK ALANLAR (Sürdürülebilirlik-Yönetim-Örnek Alan İncelemeleri). I. Kriter Yayınevi, İstanbul-Turkey, pp 51–72
72. Utlu M, Öztürk MZ, Şimşek M (2021) In: Döker MF, Akköprü E (eds) Yüksek Çözünürlüklü Sayısal Yüzey Modellerine Uygulanan Üç Boyutlu Analizler ile Kaya Düşmelerine Ait Sayısal Risk Değerlendirmesi: Ünlüyaka Köyü (Niğde, Türkiye). COĞRAFYA ARAŞTIRMALARINDA COĞRAFİ BİLGİ SİSTEMLERİ UYGULAMALARI II. I. PEGEM AKADEMi, Ankara-Turkey, pp 51–69
73. Valkaniotis S, Papathanassiou G, Ganas A (2018) Mapping an earthquake-induced landslide based on UAV imagery; case study of the 2015 Okeanos landslide, Lefkada, Greece
74. Varnes DJ (1978) Slope Movement Types and Processes.Transportation Research Board Special Report:11–33
75. Vo DT (2015) RAMMS:: Rockfall versus Rockyfor3D in rockfall trajectory simulations at the Community of Vik, Norway Dam Thanh Vo RAMMS :: Rockfall versus Rockyfor3D in rockfall trajectory simulations at the Community of Vik, Norway. University of Oslo, Faculty of Mathematics and Natural Sciences
76. Volkwein A, Schellenberg K, Labiouse V, Agliardi F, Berger F, Bourrier F, Dorren LKA, Gerber W, Jaboyedoff M (2011) Rockfall characterisation and structural protection - A review. Nat Hazards Earth Syst Sci 11:2617–2651
77. Youssef AM, Pradhan B, Al-Kathery M, Bathrellos GD, Skilodimou HD (2015) Assessment of rockfall hazard at Al-Noor Mountain, Makkah city (Saudi Arabia) using spatio-temporal remote sensing data and field investigation. J Afr Earth Sc 101:309–321
78. Žabota B, Mikoš M, Kobal M (2021) Rockfall Modelling in Forested Areas: The Role of Digital Terrain Model Grid Cell Size. Appl Sci 11:1461
79. Zhang L (2006) Rock discontinuities. In: Zhang L (eds) Engineering properties of rocks, 4th edn. Elsevier, A. Pages 226–230 *in* L. Zhang, editor. Elsevier. 4th edition. Elsevier, Amsterdam
80. Zhang Y, Yue P, Zhang G, Guan T, Lv M, Zhong D (2019) Augmented Reality Mapping of Rock Mass Discontinuities and Rockfall Susceptibility Based on Unmanned Aerial Vehicle Photogrammetry.

Figures

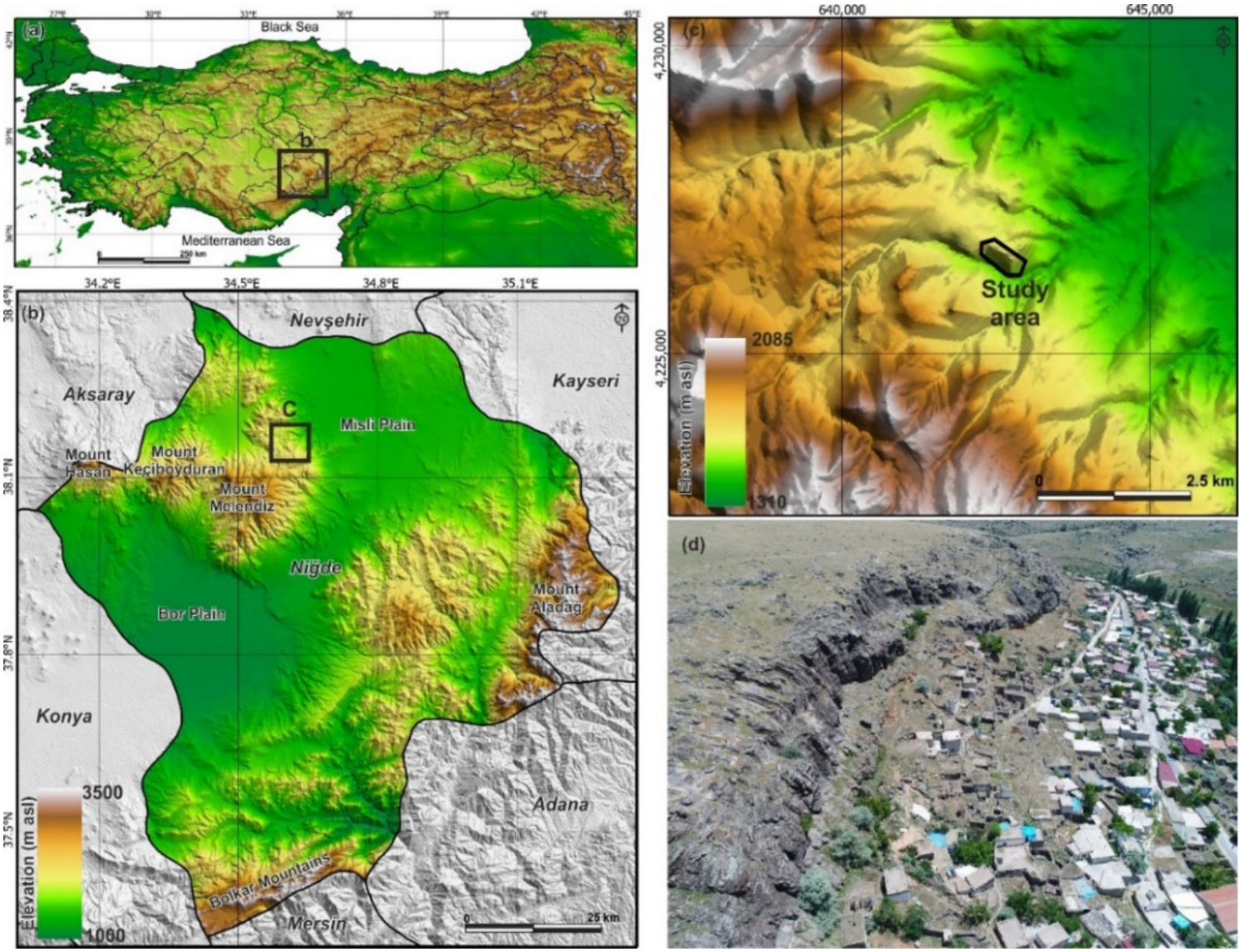

Figure 1

a-c) Location of the study area and **(d)** oblique aerial photograph of the study area.

Figure 2

General views of the village and falling rock blocks

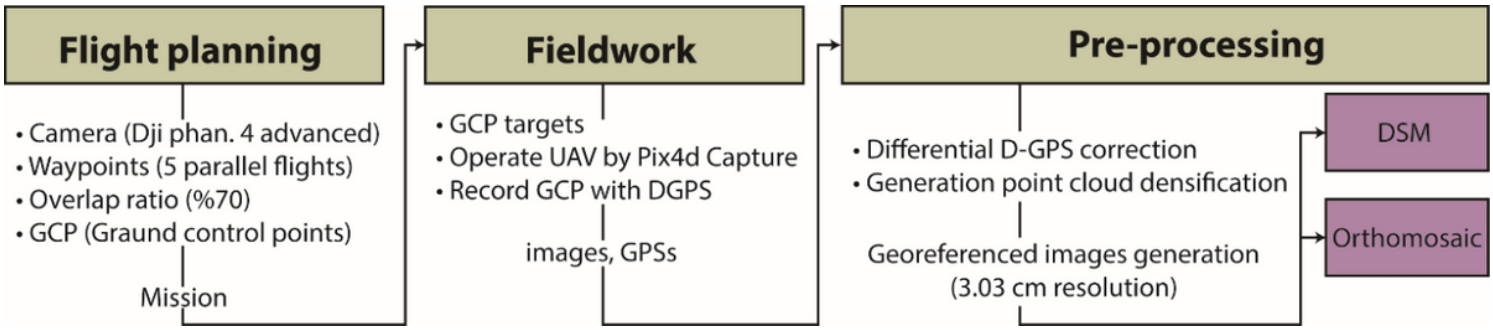

Figure 3

General flowchart for DSM and orthomosaic generation steps

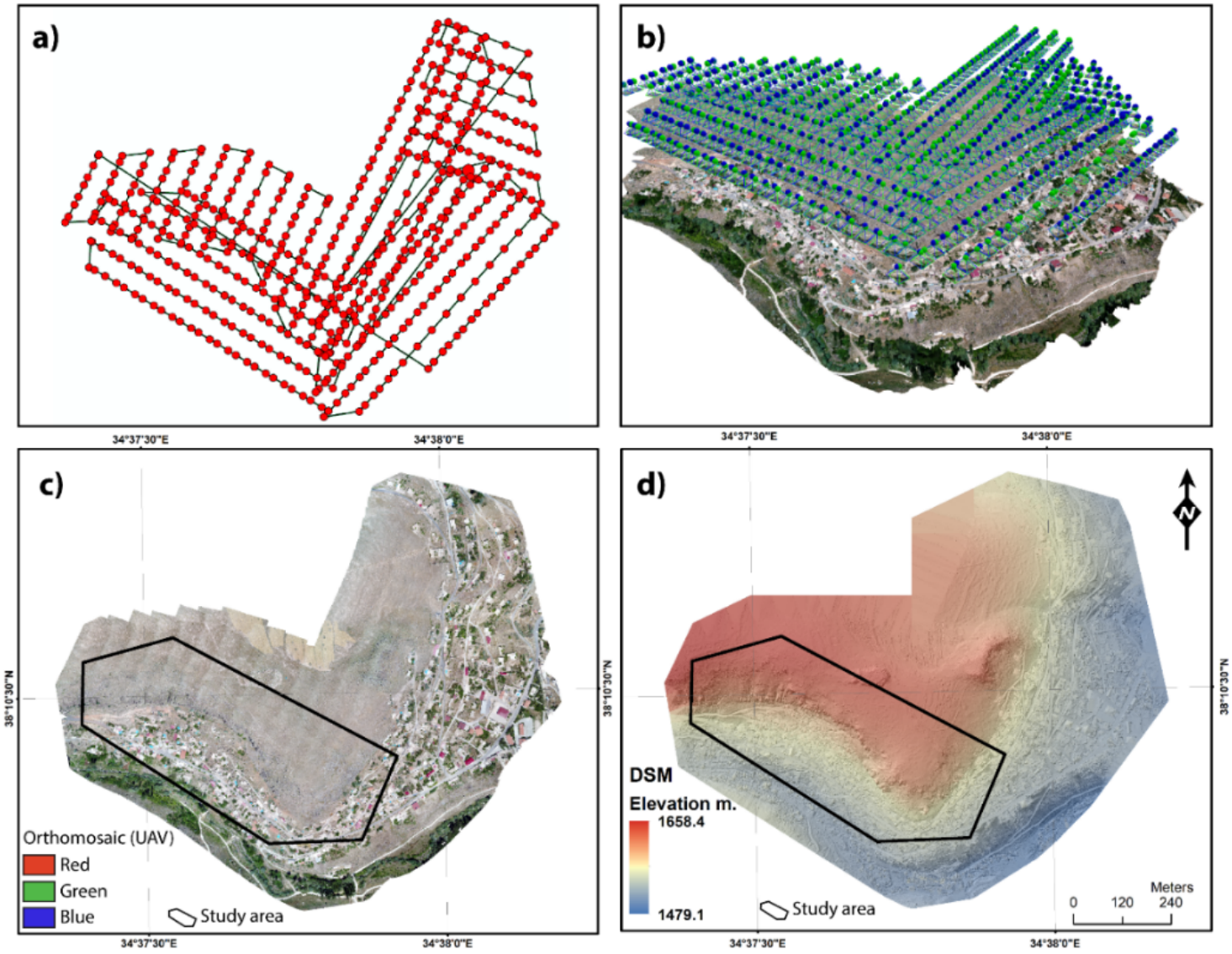

Figure 4

a) Obtaining stereo images of the planned flight path and location **b)** view represents the area of each image taken along the flight path and point cloud **c)** The orthomosaic images obtained from photogrammetric processing **d)** Digital surface model of the study area (3 cm resolution).

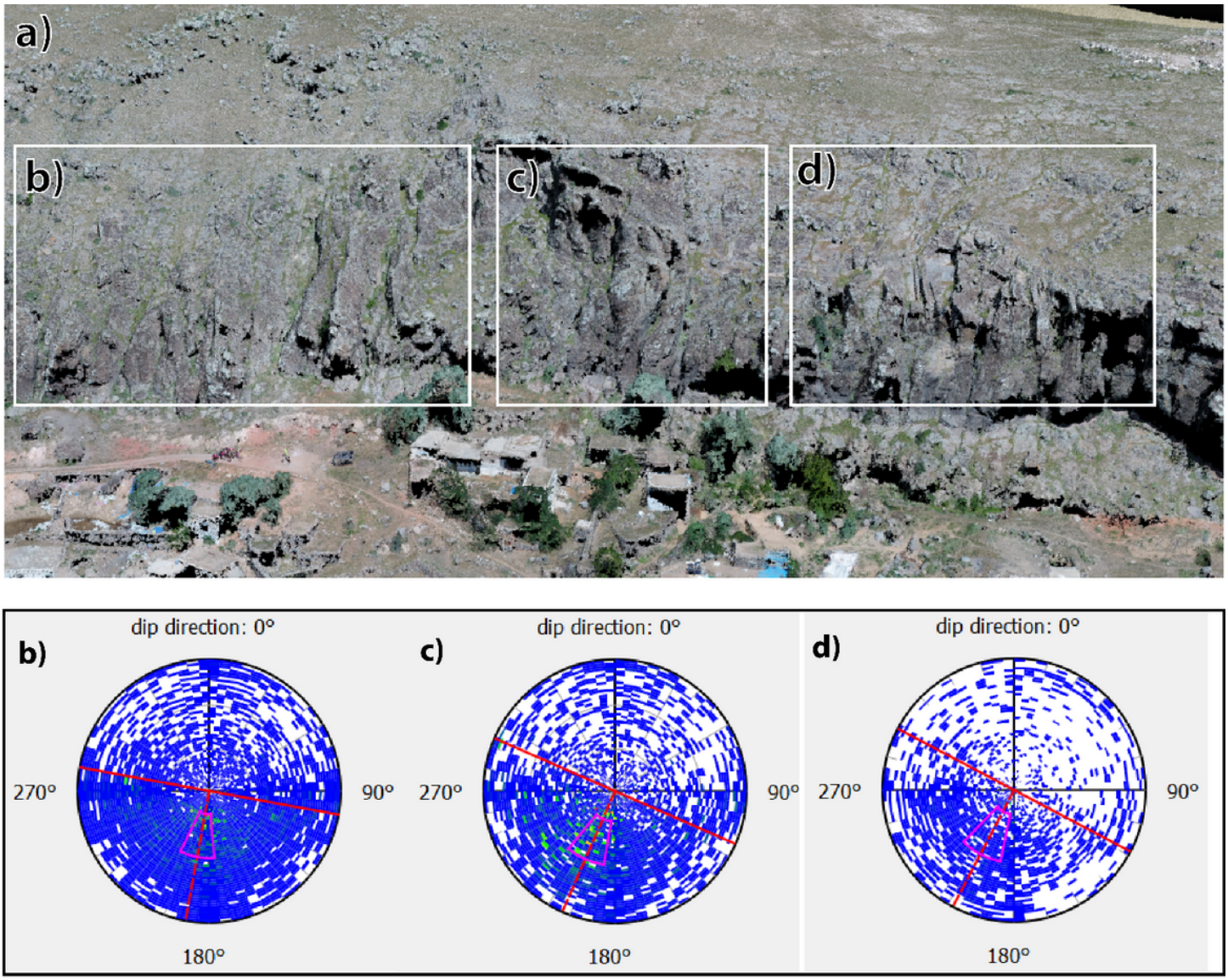

Figure 5

(a) Locations of discontinuity analysis and (b,c,d) the stereograms of facets

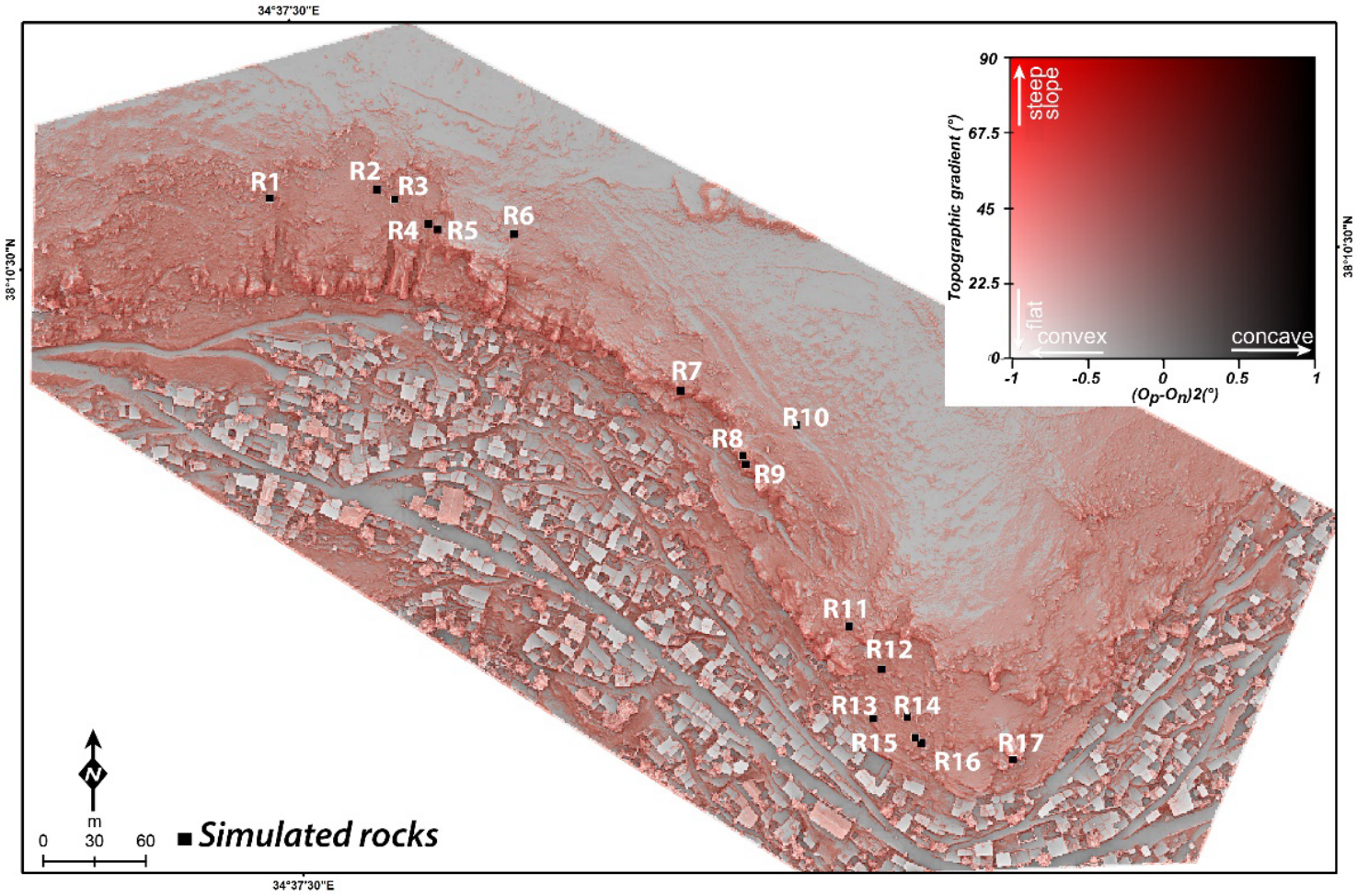

Figure 6

Red Relief Image Map (RRIM) of the study area and distribution of rock blocks have high fall risk

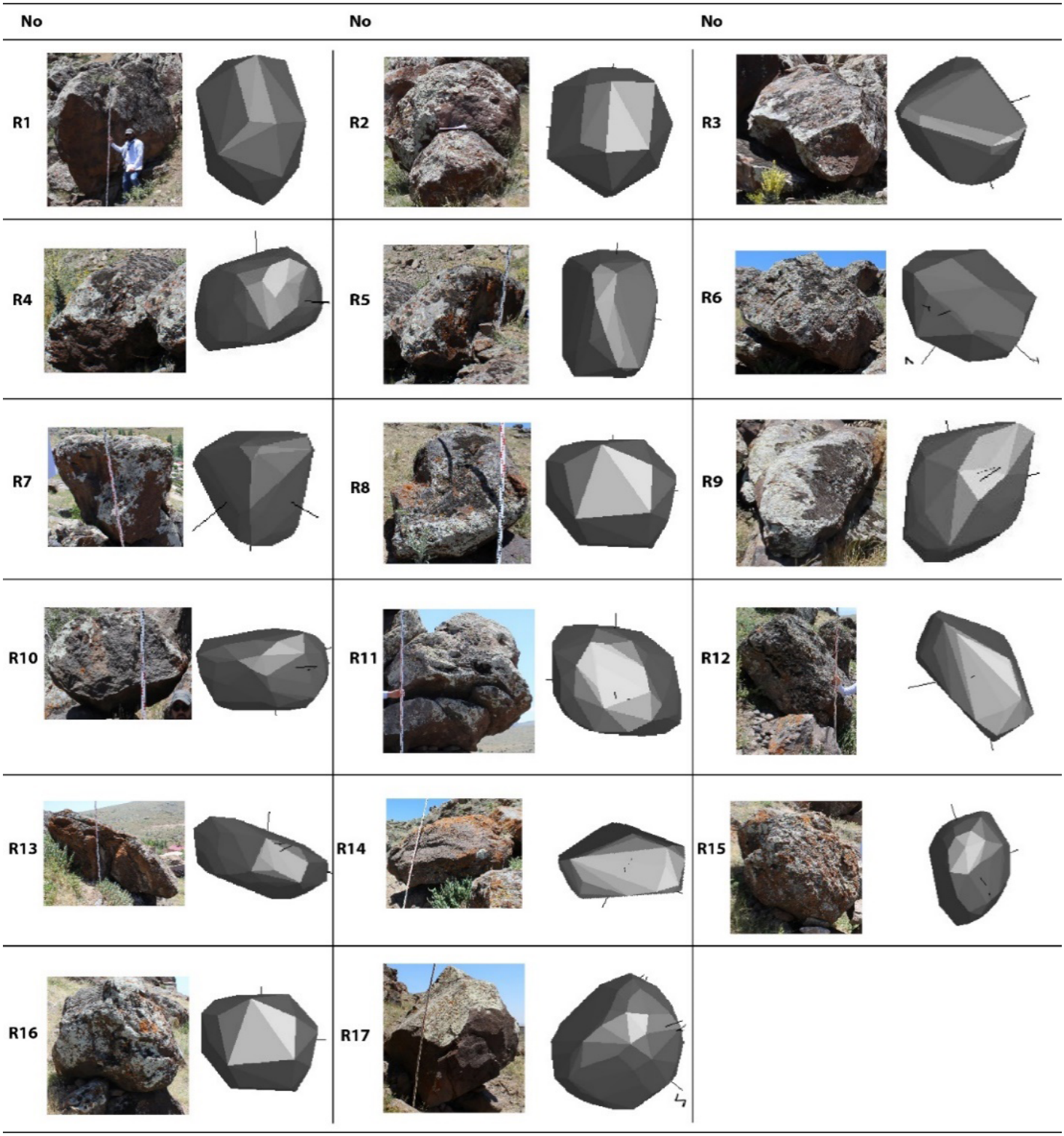

Figure 7

Photographs of rocks identified in field studies and model forms of these rocks in the RAMMS.

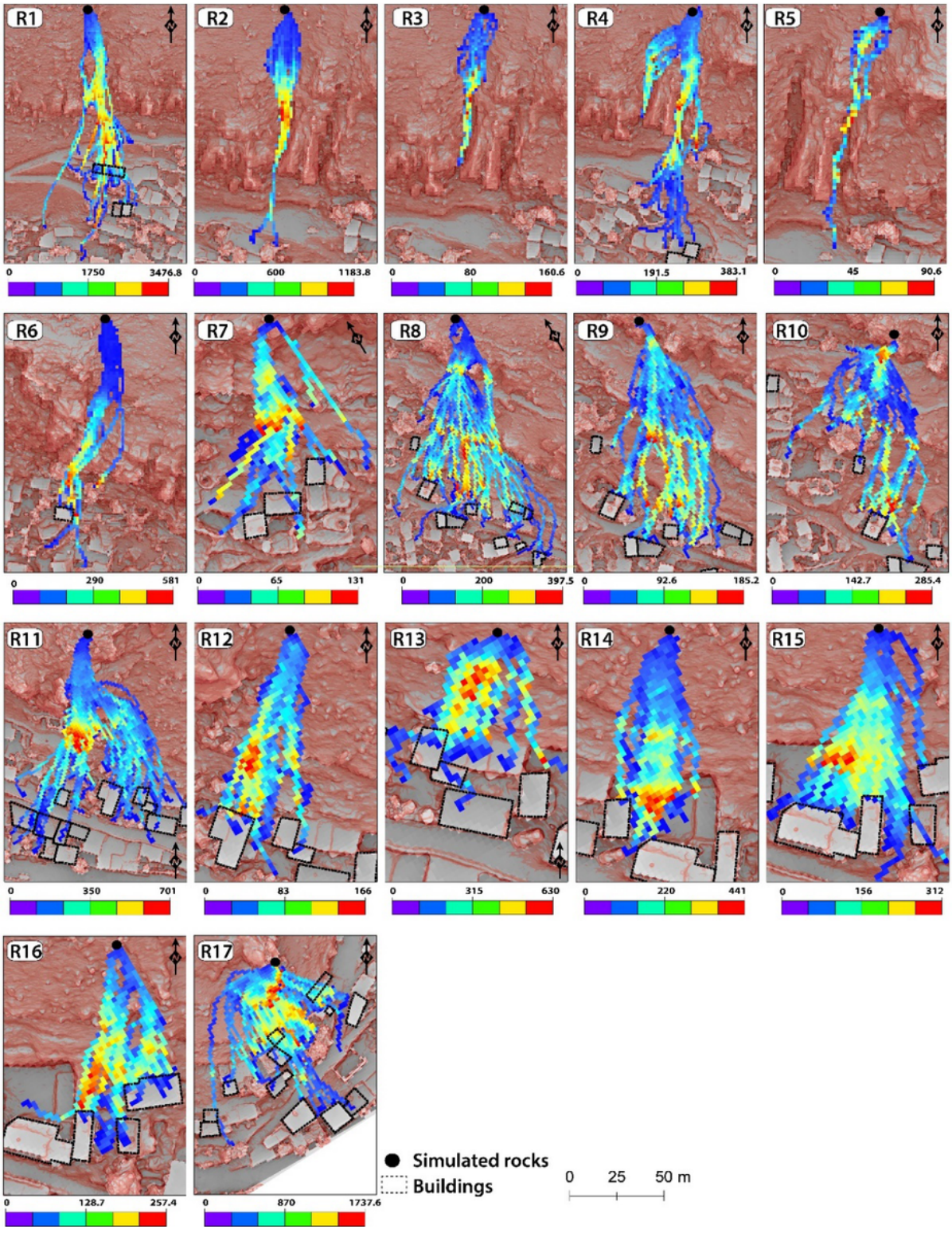

Figure 8

Rockfall trajectories and kinetic energy values of 17 blocks

Figure 9

Several views of the study area affected by rockfall events occurred in the past

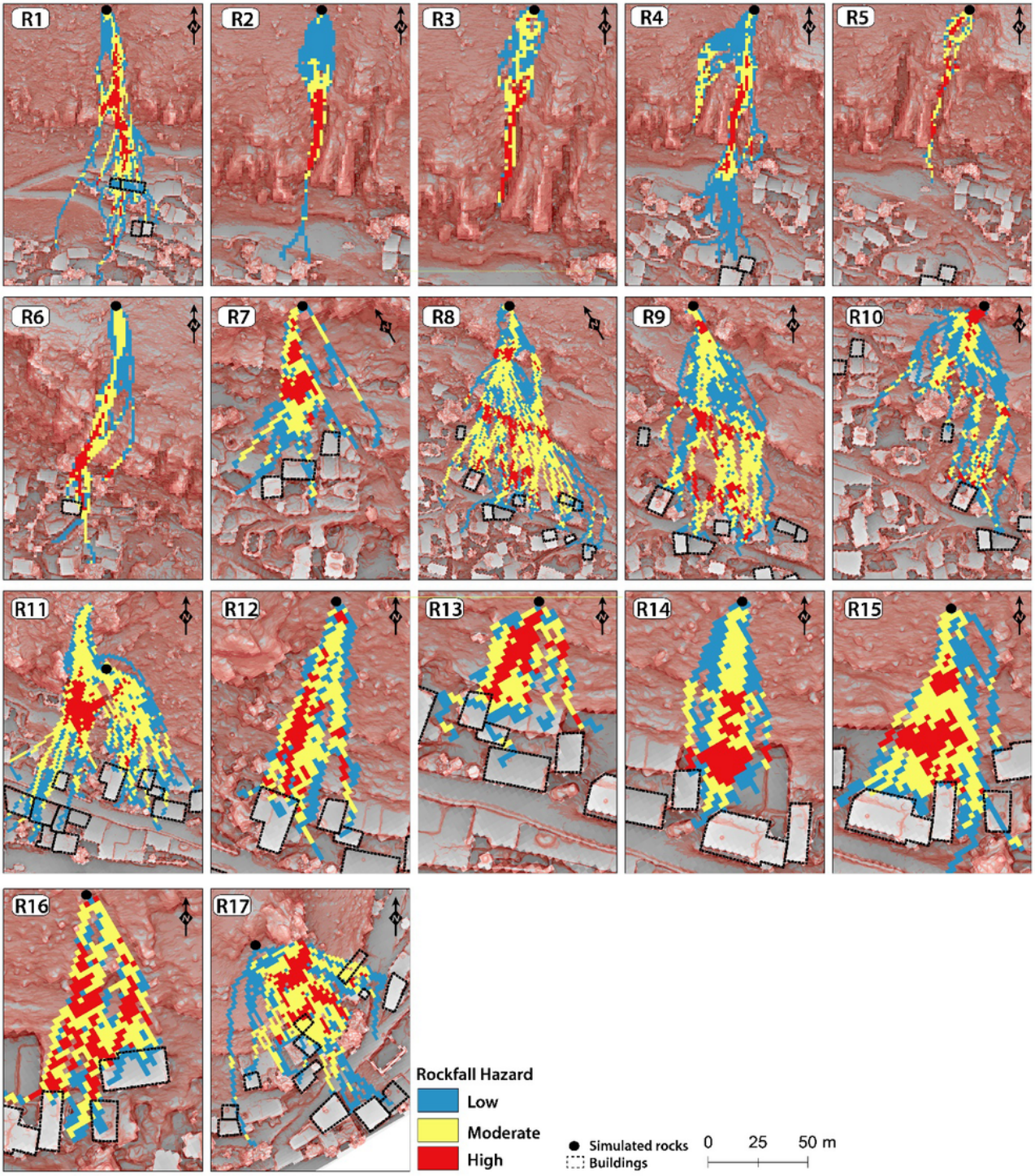

Figure 10

Rockfall Hazard Index for hanging block.

Supplementary Files

This is a list of supplementary files associated with this preprint. Click to download.

- Graphicalabstract.docx